

Atomic Velocity Projection Method: A New Analysis Method for Vibrational Spectra in Terms of Internal Coordinates for a Better Understanding of Zeolite Nanogrowth

Marc Van Houteghem,[†] Toon Verstraelen,[†] Dimitri Van Neck,[†] Christine Kirschhock,[‡] Johan A. Martens,[‡] Michel Waroquier,[†] and Veronique Van Speybroeck^{*,†}

[†]Center for Molecular Modeling, QCMM Alliance Ghent-Brussels, Ghent University, Technologiepark 903, B-9052 Zwijnaarde, Belgium

[‡]Center for Surface Chemistry and Catalysis, Leuven University, Kasteelpark Arenberg 23, B-3001 Heverlee, Belgium

 Supporting Information

ABSTRACT: An efficient protocol is presented to identify signals in vibrational spectra of silica oligomers based on theoretical molecular dynamics (MD) simulations. The method is based on the projection of the atomic velocity vectors on the tangential directions of the trajectories belonging to a predefined set of internal coordinates. In this way only contributions of atomic motions along these internal coordinates are taken into consideration. The new methodology is applied to the spectra of oligomers and rings, which play an important role in zeolite synthesis. A suitable selection of the relevant internal coordinates makes the protocol very efficient but relies on intuition and theoretical insight. The simulation data necessary to compute vibrational spectra of relevant silica species are obtained through MD using proper force fields. The new methodology—the so-called velocity projection method—makes a detailed analysis of vibrational spectra possible by establishing a one-to-one correspondence between a spectral signal and a proper internal coordinate. It offers valuable perspectives in understanding the elementary steps in silica organization during zeolite nanogrowth. The so-called velocity projection method is generally applicable on data obtained from all types of MD and is a highly valuable alternative to normal-mode analysis which has its limitations due to the presence of many local minima on the potential energy surface. In this work the method is exclusively applied to inelastic neutron scattering, but extension to the infrared power spectrum is apparent.

INTRODUCTION

Zeolites are microporous inorganic materials, mostly with aluminosilicate components, which exhibit crystal structures containing pores and cages large enough to permit the diffusion of small molecules. Zeolites are indispensable in many industrial applications, e.g., in heterogeneous catalysis, absorption and molecular separation, and ion exchange. These applications and the extension of their application field in many domains are a motivation for further investigation aiming at an even deeper insight into the behavior of a zeolite.^{1–3}

Understanding how zeolites nucleate and grow is of fundamental scientific and technological importance. Insight into the molecular mechanisms of structuring of silica can lead to the development of new hierarchical materials promising high potential for optimization of processes in catalysis and molecular separation. In addition, controlled zeolite synthesis could open new fields of application, such as optical electronics,⁴ bio-implants,⁵ etc. A variety of efforts have already been made to elucidate the early stages of zeolite growth.^{6–9} The formation of the siliceous zeolite silicalite with MFI topology is one of the best studied cases.^{10–20} Colloidal silicalite-1 is synthesized from hydrolysis of tetraethylorthosilicate (TEOS) as a monomeric silica source in aqueous tetrapropylammonium hydroxide (TPAOH) at room temperature.^{21–24} In this study we will focus on these early stages of zeolite formation from a modeling

perspective using vibrational spectroscopy: infrared (IR) and inelastic neutron scattering (INS) spectroscopy. These are important identification tools in zeolite synthesis, but the spectra are sometimes difficult to interpret. In ref 25 it was found that at the beginning of TEOS hydrolysis, small oligomers are formed which grow in number and size as the reaction progresses to form nanoparticles. Comparison between simulated and experimental IR patterns has illustrated how the silica contained in the colloidal nanoparticles evolve with time, leading from small five-ring oligomers toward successively more condensed five-ring species.^{22,24,26}

Two methods are conventionally used for the calculation of vibrational spectra linking spectral patterns with atomic motions: normal-mode analysis (NMA) based on static approaches and a Fourier-based technique which receives input from molecular dynamics (MD) simulations. NMA is computationally less demanding but is restricted to the harmonic approximation which allows only small deviations from a local or global minimum on the potential energy surface (PES). The restriction stems from the fact that NMA is in essence a second-order approximation of the minima in the PES. As a consequence, only one minimum can be calculated and just a small part of the

Received: September 20, 2010

Published: March 03, 2011

surface is taken into account, which limits the technique when multiple minima are present.²⁷ Static approaches can go beyond the harmonic approximation. We refer in particular to the work of Scribano and Benoit²⁸ where the vibrational self-consistent field method (VSCF) is combined with the single-to-all (STA) approach succeeding in the construction of a sparse PES at high ab initio levels of theory. With the second technique, data from MD simulations are used to calculate spectra. In the past many papers have already been published in literature aiming at identifying signals in the Raman or IR spectrum as signatures for specific vibrations characterizing the structure of the molecular system under study. It is not the intention to give a complete survey of all works published in this area, we limit ourselves to those related with vibrations in silica particles. In particular we refer to ref 29 as a pioneering work in which vibrational spectra have been interpreted by means of a normal-mode analysis in terms of symmetry coordinates predicted by point group theory. Other papers analyzed the vibrational eigenmodes with the help of MD to identify signals as signatures of ring structures in silica.³⁰ Their focus is mainly devoted to the description of symmetric stretching modes, such as breathing modes in rings, as these are recognized to be Raman active. The vibrational eigenmodes are projected onto the coherent breathing modes of the bridging oxygen atoms. They could in many cases provide an unambiguous interpretation for the origin of the Raman lines. Also the group of Smirnov has been very active in this domain.^{31–37} Power spectra belonging to a suitably chosen symmetric internal coordinate describing the breathing vibration of a specific ring are constructed and were found to be able to discriminate the various ring structures. To get a better insight into the participation of atoms of different types in the vibrational spectra, a power spectrum for each kind of atom was computed by Fourier transformation of the atomic velocity autocorrelation functions. Some MD techniques (e.g., ab initio MD) are computationally expensive while others are not (e.g., based on force fields). So it depends on the chosen MD method whether or not a large part of the PES can be scanned. The reliability of such numerical simulation methods to reproduce experimental results strongly depends on the method to calculate the PES. Accurate potentials are necessary to describe the atomic and molecular forces of the molecule under study and to reproduce the structural properties and dynamical data. In order to obtain a reliable spectrum it is essential to scan a large part of the PES and thus to simulate during a representative time frame (\sim ns range). In view of this, only force field-based methods are viable to calculate the PES as quantum mechanically based methods appear to be too expensive for larger systems and for longer time scales, although serious progress is made on this issue by the group of Parrinello^{38,39} by combining Car–Parrinello and Born–Oppenheimer MD. Most of the existing protocols to derive vibrational spectra from the data collected during MD simulations are applicable regardless of whether force fields or ab initio MD are used. Despite many attempts to interpret the vibrational spectra and to define the internal mode contributing to a certain band in the vibrational spectrum further model development remains desirable. Very recently Jacob and Reiher⁴⁰ developed a model in which the frequencies at which the bands in the vibrational spectra appear, and the total intensities of these bands can be interpreted in terms of localized modes. This method seems to be very appropriate in analyzing spectra of large molecules like polypeptides and proteins, but the protocol is constrained to static quantum chemical calculations.

In this paper we present a completely new methodology for the interpretation of vibrational spectra but based on molecular dynamical approaches. In the new model the atomic velocities are projected on properly selected directions fully determined by the internal mode from which we want to know its impact on the spectrum. Numerical applications of the new method are based on classical MD simulations. For the silica building blocks under investigation in this work, we use a silica-derived force field based on the gradient curves method⁴¹ which was previously successfully applied to investigate the MFI fingerprint in zeolites.²⁶

The infrared power spectrum is computed by taking the Fourier transform of the autocorrelation function of the time variation of the electric dipole moment. Similarly, the velocity power spectrum or INS spectrum is determined by the Fourier transform of the atomic velocities, which is easier to compute after a MD run as it only needs the instantaneous atomic velocities at each time step. Compared to NMA, this dynamical approach is more flexible in the treatment of nonharmonic problems, although also in static approaches progress is made in going beyond the harmonic approximation as already stated.

The first goal of this paper is to identify peaks in vibrational spectra of zeolite building blocks with specific internal degrees of freedom. In particular we were interested in how the size of rings and/or connectivity affects signals in the vibrational spectrum. For this purpose a new method has been developed enabling us to link the spectrum with the internal degrees of freedom of zeolite nanoparticles. This method provides a suitable tool that predicts which particular modes are influenced by changing size and topology of the silica building blocks. As such, it constitutes a significant progress in understanding the mechanisms during the early stages of the zeolite growth, and it gives complementary and valuable information in addition to the usual protocol of spectra analysis where experimentally measured spectra are compared with fully theoretical spectra extracted from simulations of the zeolite frameworks.^{34–37,42} The basic understandings of zeolite spectra and the lattice dynamics of zeolites are well-known.^{43–45} But a computational method for an unambiguous validation and confirmation of peak assignments in smaller silica particles can still be improved. In addition, it can in turn be helpful in the development and/or refinements of models to compute atomic forces, e.g., force fields. If a MD run does not yield the correct vibrational spectrum with regard to experiment, in the sense that some peaks are missing or not at the correct position, the new methodology makes it possible to specify the internal mode that is poorly described. Relevant terms in the force field can be adjusted accordingly to remove the discrepancies.

In ref 26 the MFI topology was studied in terms of shifts of peaks as MFI-structured nanoparticles grow. As the particles become bigger in size, the fingerprint band lowers in frequency from 650 to 550 cm⁻¹. An isolated five-membered ring (5T) reveals an IR-active vibration around 650 cm⁻¹. By connecting pentasil rings, slightly larger building blocks are constructed, but no substantial changes for the peak position have been observed. The situation changes if a more condensed structure is formed, such as the silica octamer, referred to as 8T (4 × 5) (see Figure 11); a sudden shift by approximately 50 cm⁻¹ is observed. The red shift becomes even more substantial when the particles grow larger. This 550 cm⁻¹ band is regarded as the spectroscopic

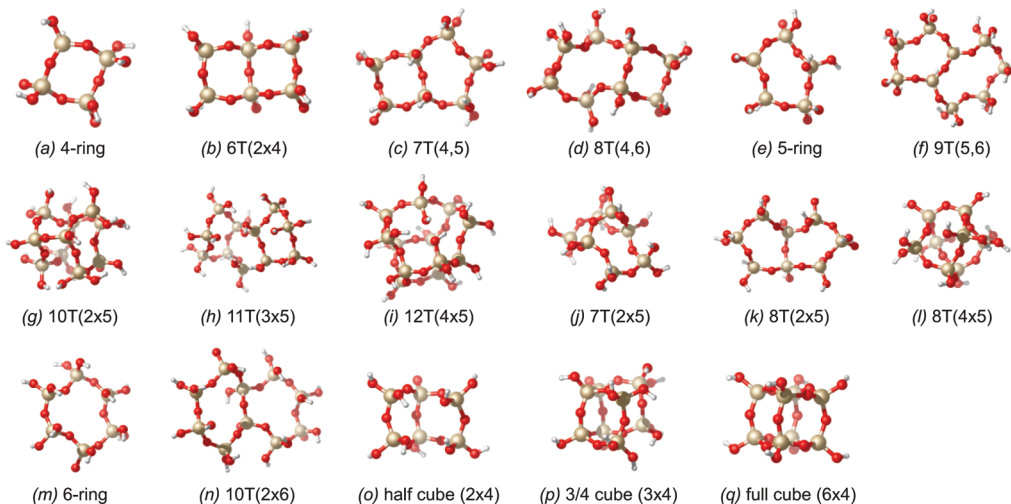


Figure 1. Simulated molecular structures of silica particles consisting of combinations between various four-, five-, and six-rings.

signature of MFI-type zeolites and is also a typical feature of similar structures built from five-membered rings, the so-called pentasil zeolites.

In this paper we apply a new methodology—the so-called velocity projection method—to a large variety of building blocks encountered in zeolite synthesis, including four-, five-, and six-rings and all types of connections between them (Figure 1). The analysis presented here should serve as a basic understanding of which modes and which peaks in the vibrational spectra are influenced by the particular interconnectivity and topology. The lack of experimental vibrational spectra of such small silica particles in the literature strengthens the importance of such a theoretical investigation. For larger species experimental data are available.

■ COMPUTATIONAL SECTION

The input of the computed spectra is generated from MD simulations. Interatomic interactions between framework atoms were represented by an in-house developed force field. It was especially designed for zeolites and was calibrated at the post-Hartree–Fock MP2/6-311+g(d,p) level of theory, with the gradient curves method (GCM).⁴¹ This is a novel technique that facilitates the development of transferable force-field models. It makes extensive use of regularization techniques⁴⁶ and of generic energy terms based on series expansions to obtain an optimal bias–variance trade-off during the fitting procedure. The force field was previously thoroughly benchmarked to reproduce the MFI fingerprint and IR-band shifts in other related small silica nanoparticles. All optimizations and simulations have been carried out with the CP2K⁴⁷ program package.²⁶

All initial geometries were built with the in-house developed software program package ZEOBUILDER.⁴⁸ Geometry optimizations were performed on all structures using the conjugate gradient method. With these optimized coordinates as input, an initial equilibration MD run of 5 ps was carried out. The actual production run which provided the data for analysis was an MD run of 1 ns at a temperature of 300 K with a Nose thermostat in the NVT statistical ensemble. To process the data, the MD-TRACKS program⁴⁹ was used.

From linear response theory, if the dipole moment history is obtained in an MD calculation, then the infrared spectrum $I_{\text{IR}}(\omega)$ can be computed as^{50–53}

$$I_{\text{IR}}(\omega) = \lim_{t \rightarrow \infty} \frac{1}{t} \sum_{\alpha=x,y,z} \left| \int_0^t \frac{d\mu_\alpha}{dt} \exp(-i\omega t) dt \right|^2 \quad (1)$$

where ω is the angular frequency, and μ_α is the Cartesian components of the dipole moment. This is equivalent to the Fourier transform of the autocorrelation function of the time derivative of the dipole moment.^{53,54} The dipole moment is defined as

$$\boldsymbol{\mu} = - \int (\mathbf{r} - \mathbf{R}_c) \rho(\mathbf{r}) d\mathbf{r} + \sum_{i=1}^N Z_i (\mathbf{R}_i - \mathbf{R}_c) \quad (2)$$

where $\rho(\mathbf{r})$ is the electron density, Z_i represents the nuclear charge of atom i , \mathbf{R}_i is the position of atom i , and N the total number of atoms. The reference point \mathbf{R}_c is the center of charge for charged systems and is arbitrary for neutral systems. In molecular mechanics, one preferentially uses an effective charge Q_i for each atom, and the dipole moment is written as

$$\boldsymbol{\mu} = \sum_{i=1}^N Q_i (\mathbf{R}_i - \mathbf{R}_c) \quad (3a)$$

$$\frac{d\boldsymbol{\mu}}{dt} = \sum_{i=1}^N Q_i \mathbf{v}_i \quad (3b)$$

In this work fixed charges were used. The velocity power spectrum or inelastic neutron scattering spectrum (INS) can be obtained in a similar way as the infrared signal using an autocorrelation function:

$$I_{\text{INS}}(\omega) = \lim_{t \rightarrow \infty} \frac{1}{t} \sum_{i=1}^N \left| \int_0^t \mathbf{v}_{i,\alpha}(t) \exp(-i\omega t) dt \right|^2 \quad (4)$$

$\alpha=x,y,z$

The IR and INS spectra are based on a Fourier transform which transforms information from the time domain to the frequency domain. One can easily see that both spectra are directly dependent on the velocities of the atoms $R_{i\alpha} = v_{i\alpha}$ so that the positions of peaks in IR and INS spectra coincide, but the intensities will vary.

The Fourier transform of the velocity autocorrelation provides information about the density of vibrational modes as a function of energy and hence reveals the underlying frequencies of the molecular system. The IR spectrum shows which internal modes are infrared active. If some of the IR active modes are localized on specific functional groups, then the corresponding bands can then serve as a spectral fingerprint of the groups. However, we focus in this paper on the INS spectra since charges in force fields are not (yet) well-defined in order to obtain reliable qualitative spectral amplitudes. Moreover, cancellation effects frequently appear in the time-varying dipole moment vector (eq 3a). It implies that the amplitudes in an IR spectrum are smaller and faster affected by relative noise. On the contrary, the INS spectrum contains only a summation of positive contributions (eq 4), and the relative noise on the spectrum becomes smaller. It also provides information about all vibrations of the system, i.e., all IR and Raman active modes.

METHOD

Velocity Projection Method. In order to associate peaks in the full INS spectrum to particular motions of internal coordinates we developed a method where the atomic velocities are projected to selective directions defined by the specific nature of the internal coordinate. An outline of this projection method is sketched below.

We make use of internal coordinates in order to assign a peak to one particular degree of freedom. An internal coordinate (IC) defines the location of the atoms in a molecule relative to the other atoms in the molecule. Some examples of IC's are bond distances, bending angles, dihedrals, Urey–Bradley stretches,⁵⁵ a linear combination of stretches, etc. Each internal coordinate q can be expressed as a function of the atomic Cartesian coordinates $R_{i\alpha}$ and depends on time: $q = q(R_{i\alpha}(t))$. The velocity projection method then consists of projecting the Cartesian velocity vector $v_{i\alpha} = \dot{R}_{i\alpha}$ of each atom i on the atomic tangent vector of the internal coordinate q at each time step. The IC's themselves are overcomplete and are, in contrast with NMA, not orthogonal to each other. In this section, the different classes of IC's that were used in this work will be illustrated. If one considers only one IC, then the definition of the tangent vector of atom i at each time step is given by

$$J_{i\alpha} = \frac{\partial q}{\partial R_{i\alpha}} \quad (5)$$

where α runs over the Cartesian x , y , and z components of atom i . Obviously, i must be one of the atoms that specifies the IC $q(R_{i\alpha})$. The velocity vector belonging to atom i can be decomposed into its tangential and normal component with respect to the atomic tangent vector $J_{i\alpha}$:

$$v_{i\alpha} = (v_{\perp})_{i\alpha} + (v_{//})_{i\alpha} \quad (6)$$

Only the tangential component gives a nonvanishing contribution to the change of the internal coordinate:

$$\delta q = \sum_i J_i \cdot \delta R_i \quad (7)$$

and with a suitable normalization can be set as

$$(v_{//})_{i\alpha} = \frac{(\sum_{j\beta} v_{j\beta} J_{j\beta}) J_{i\alpha}}{\sum_{j\beta} J_{j\beta}^2} \quad (8)$$

while the normal component lets the IC unchanged in first order (for small time steps):

$$(v_{\perp})_{i\alpha} = v_{i\alpha} - (v_{//})_{i\alpha} \quad (9)$$

The parallel velocity is the component that should be identified with this particular internal coordinate. Note that the IC is a function of time, and we project on a time dependent vector. To compute the actual spectrum, the Cartesian components of the velocities of every atom at each time step are plugged into eqs 1 and 4. The fluctuations due to the time dependency of the IC's are also computed with the Fourier transformation but should be small enough to neglect. Accordingly, an autocorrelation function (eq 4) is computed with the instantaneous $(v_{//})_{i\alpha}$ velocity projections. In this way a partial INS spectrum has been constructed restricted to those vibrations inducing changes of the IC of interest. A comparison between the full and partial INS spectra makes a full analysis of the vibrational spectrum possible: spectral peaks can be linked to IC's and corresponding (internal) degrees of freedom. When a peak in the projected spectrum coincides with its counterpart in the total spectrum, one can assume that there is no motion along other orthogonal coordinates that contributes to this peak. Such a peak is then completely resolved.

We note that the normalization of the tangential component (eq 8) is not unique and that a separate projection of the atomic velocity to the tangent vector belonging to that atom leads to a somewhat different normalization factor:

$$(v_{//})_{i\alpha} = \frac{(\sum_{i\beta} v_{i\beta} J_{i\beta}) J_{i\alpha}}{\sum_{i\beta} J_{i\beta}^2} \quad (10)$$

For computational reasons we have given preference to the normalization in (eq 8) to avoid numerical inaccuracies generated by tangent vectors J_i of very small amplitude, as would be the case with the choice of solution 10.

Internal Coordinates. Analysis Using Internal Coordinates. At this point it is useful to outline the exact workflow. The standard procedure to obtain a vibrational spectrum from MD data is to compute the Fourier transform of the Cartesian atomic velocities (eqs 1 and 4) at each time step. In this work we project the Cartesian atomic velocities onto IC's to obtain the velocity component $(v_{//})_{i\alpha}$ of each atom alongside the IC (eq 8 and eq 9). Of these projected velocities, which are by definition equal to or smaller than the atomic Cartesian velocities, the Fourier transform is also computed at each time step to obtain the spectrum of the velocities for each IC separately. It can happen that, due to symmetry, some classes of IC's generate almost identical spectra; then the average was taken over them. In the next section the different classes of internal coordinates that were used in this work are discussed.

Classes for Internal Coordinates. The peaks in the full spectra can be (partially) decomposed by a proper selection of IC's. This can be done for the various zeolite building blocks under study in

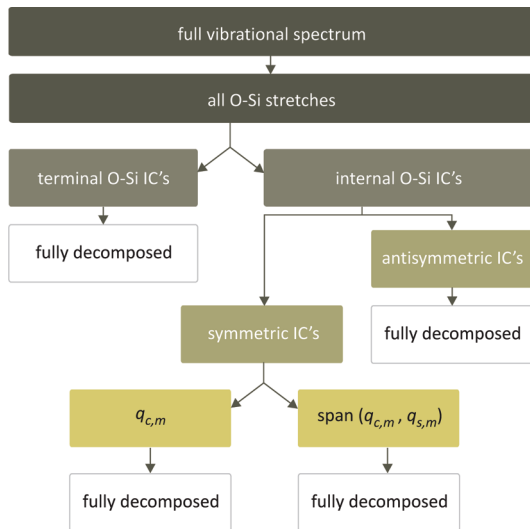


Figure 2. Flowscheme to classify different IC's used to decompose vibrational zeolite spectra.

this work and displayed in Figure 1. The IC's or linear combinations of them are then classified. Each class has its specific internal motion and generates a partial INS spectrum for each building block.

We will follow the following protocol. For all structures we compute the full vibrational spectrum based on the (nonprojected) atomic velocities as resulting from the MD simulation. For each individual IC we then project the atomic velocities according to the outlined procedure trying to link spectral peaks to these IC's. Linear combinations of various IC's can be constructed to form new IC's. With a well-chosen linear combination, one is able to fully assign a peak to this new specific internal coordinate. The general workflow for combining IC's to further unravel the spectra and to be able to link them with a spectral peak is shown in Figure 2. In this paper we focus on IC's constructed from stretches between two atoms: the stretches themselves can serve as IC's or linear combinations of them. The stretching vibration is one of the most straightforward internal motions to describe. In an earlier study by van Santen et al.,⁴⁵ it was stated that the lattice dynamics of amorphous silica can be correctly described by ignoring the Si—O—Si bending and solely focusing on the Si—O stretchings (see Figure 3). It implies that the wavenumber regime of 500–1200 cm⁻¹ is sufficient for studying the zeolite nanogrowth. As the studied species are however much smaller, we will validate in how far only stretches are applicable for fully resolving the spectrum. The higher the connectivity, the higher the rigidity and thus preventing the bending mode. Mixing of the Si—O stretching and Si—O—Si bending modes in the case of small oligomers may be assumed to be of minor importance because their modes are spectrally well separated.

Looking at Figure 3 we can discriminate between two types of O—Si stretches. The first one is the stretch mode, which occurs along the O—Si bond, where the oxygen atom is connected with a terminal hydrogen atom. This will be referred to as the O—Si terminal stretch. The second type consists of the two O—Si stretches in the Si—O—Si bridge. Such O—Si stretch is called an internal O—Si stretch. We make an approximation in the sense that the interaction between the symmetric and antisymmetric modes can be neglected, which is quite reasonable in view of the

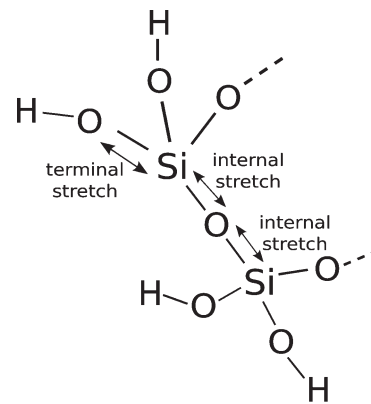


Figure 3. Schematic representation of the Si—O stretches present in the studied zeolite structures.

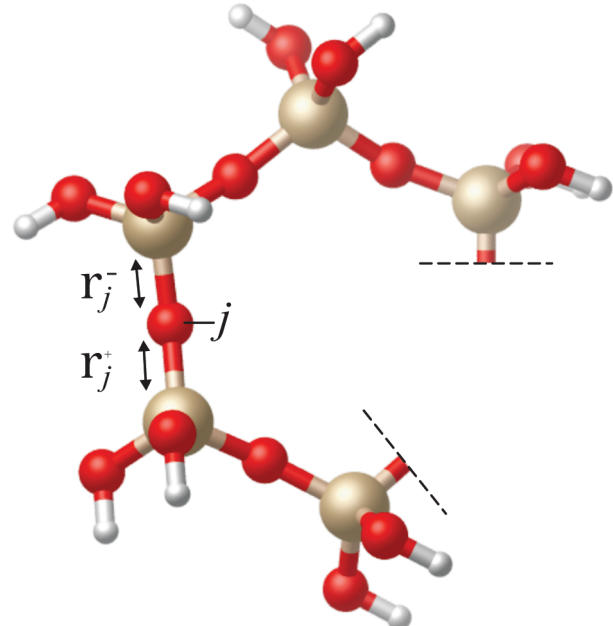


Figure 4. Ring stretching Si—O bonds defining symmetric and antisymmetric IC's.

large difference between the spectral values of these modes and the magnitude of the coupling constant.⁴⁵

One can choose a particular Si—O stretch as IC, but in practice, linear combinations of stretch modes are more appropriate choices for IC's. In this way we separate the $2N$ ring stretching Si—O bonds, present in a N -membered ring, into two classes of IC's (symmetric and antisymmetric). For one particular Si—O—Si bridge j :

$$q_{ss,j} = \frac{1}{\sqrt{2}}(r_j^- + r_j^+) \quad (11)$$

and

$$q_{as,j} = \frac{1}{\sqrt{2}}(r_j^- - r_j^+) \quad (12)$$

as visualized in Figure 4 .

The coordinate transformation between all stretching internal coordinates and the N symmetric and antisymmetric IC's is orthogonal and of dimension $2N \times 2N$:

$$\begin{bmatrix} \mathbf{q}_{ss} \\ \mathbf{q}_{as} \end{bmatrix} = \mathbf{T} \mathbf{r} \quad (13)$$

$\mathbf{r} = (2N \times 1)$ matrix (Si – O stretches)

$\mathbf{T} = 2N \times 2N$ matrix and orthogonal

The force constant matrix in $\{\mathbf{q}_{ss}, \mathbf{q}_{as}\}$ space becomes

$$\mathbf{U} = \frac{1}{2} (\mathbf{q}_{ss}^T \mathbf{q}_{as}^T) \mathbf{C}_q \begin{bmatrix} \mathbf{q}_{ss} \\ \mathbf{q}_{as} \end{bmatrix} \quad (14)$$

with $\mathbf{C}_q = \mathbf{T} \mathbf{C}_r \mathbf{T}^T$, which is not block diagonal even with a diagonal structure of \mathbf{C}_r :

$$\mathbf{C}_q = \begin{bmatrix} \mathbf{C}_{q_{ss}} & \mathbf{C}_{q_{coupl}} \\ \mathbf{C}_{q_{coupl}} & \mathbf{C}_{q_{as}} \end{bmatrix} \quad (15)$$

In the model proposed it is assumed that the coupling between the symmetric and antisymmetric stretch modes is very weak and may be omitted: $\mathbf{C}_{q_{coupl}} = 0$. This seems to be justified since the frequency bands of both classes are well separated, as will be demonstrated later in the discussion section.

It is interesting to examine the symmetric stretch mode in more detail. The peaks due to the symmetric stretch are not completely resolved, and they lie in the wavenumber region which is interesting for obtaining insight into zeolite synthesis (the antisymmetric stretch peaks are completely resolved and lie in a less interesting area). In order to gain insight into the normal (symmetric stretch) modes of a molecular ring system, we consider a simplified model of n identical and equally spaced masses on a circle. Due to its periodicity, the normal modes of such a system can be obtained as the eigenvectors of a so-called circulant matrix C :

$$C_{jk} = c_{(j-k) \bmod n} \quad (16)$$

for $j, k = 1, \dots, n$, where the notation $(i) \bmod n$ implies integer arithmetic modulo n . Since the Hessian of the model system is a symmetric matrix ($C_{jk} = C_{kj}$), the coefficients must also obey

$$c_{(i) \bmod n} = c_{(-i) \bmod n} \quad (17)$$

where we used the notation $-i = n - i$. The circulant matrix C for an even n then has the form:

$$C = \begin{bmatrix} c_0 & c_1 & \dots & c_{n/2} & c_{n/2-1} & \dots & c_1 \\ c_1 & c_0 & \dots & & & & \\ \vdots & & \ddots & & & & \\ c_{n/2} & & & \ddots & & & \\ c_{n/2-1} & & & & \ddots & & \\ \vdots & & & & & \ddots & \\ c_1 & & \dots & & c_1 & & c_0 \end{bmatrix} \quad (18)$$

The form of C for n being odd is analogous. In the remainder we drop the explicit "mod n " notation for the $c_{(i)}$ indices, but it is understood that they should be interpreted in arithmetic modulo n . The eigenvectors of the circulant matrix can be used to create new IC's on which we can project the atomic velocities, based on

the symmetric stretch IC's $q_{ss,k}$. With the circulant matrix being the model for the Hessian, we can construct these new internal coordinates, i.e., linear combinations of symmetric stretches, to further resolve the spectra of silica rings.

The eigenvalues and the k^{th} component of the normalized eigenvectors are (see Appendix Section):

$$\begin{aligned} \lambda^{(m)} &= \sum_k c_{(k)} \exp\left(\frac{-2\pi imk}{n}\right) \\ &= \sum_k c_{(k)} \cos\left(\frac{2\pi mk}{n}\right) = \lambda^{(-m)} \end{aligned} \quad (19)$$

and

$$V_k^{(m)} = \frac{1}{\sqrt{n}} \exp\left(\frac{2\pi imk}{n}\right) \quad (20)$$

Looking at the eigenvalue spectrum one can distinguish between even n (four-, six-ring, etc.) and odd n (five-ring, etc.). For even n the eigenvalues (eigenvectors) become

$$\begin{cases} \lambda^{(0)}(V^{(0)}) : \text{nondegenerate} \\ \lambda^{(m)}(V^{(m)}, V^{(-m)}) \text{ for } m = 1, \dots, \frac{n}{2} - 1 : \text{two-fold degenerate} \\ \lambda^{(n/2)}(V^{(n/2)}) : \text{nondegenerate} \end{cases}$$

For odd n they are

$$\begin{cases} \lambda^{(0)}(V^{(0)}) : \text{nondegenerate} \\ \lambda^{(m)}(V^{(m)}, V^{(-m)}) \text{ for } m = 1, \dots, \frac{n-1}{2} : \text{two-fold degenerate} \end{cases}$$

It is practical to switch to real eigenvectors for the two-fold degenerate eigenspaces, by taking linear combinations:

$$W_k^{(m)} = \frac{1}{2} (V_k^{(m)} + V_k^{(-m)}) = \cos\left(\frac{2\pi}{n} mk\right) \quad (21a)$$

$$W_k^{(-m)} = \frac{1}{2i} (V_k^{(m)} - V_k^{(-m)}) = \sin\left(\frac{2\pi}{n} mk\right) \quad (21b)$$

It is now possible to construct a new internal coordinate for each eigenvector m by making linear combinations of the symmetric stretches $q_{ss,k}$ where the coefficients are the elements of the eigenvector. For the circular systems under consideration, the new internal coordinates become

$$\begin{aligned} q_{c,m} &= \sum_k W_k^{(m)} q_{ss,k} = \sum_k \frac{V_k^{(m)} + V_k^{(-m)}}{2} q_{ss,k} \\ &= \sum_k \cos\left(\frac{2\pi}{n} mk\right) q_{ss,k} \end{aligned} \quad (22a)$$

$$\begin{aligned} q_{s,m} &= \sum_k W_k^{(-m)} q_{ss,k} = \sum_k \frac{V_k^{(m)} - V_k^{(-m)}}{2i} q_{ss,k} \\ &= \sum_k \sin\left(\frac{2\pi}{n} mk\right) q_{ss,k} \end{aligned} \quad (22b)$$

where n is the number of symmetric stretches in the circular molecular system and $q_{ss,k}$ is short for the k^{th} symmetric stretch IC. Since $q_{c,m}$ and $q_{s,m}$ only differ in phase we could not discriminate between them. Therefore it is useful to consider the subspace spanned by these vectors. This subspace is referred to as $\text{span}(q_{c,m}, q_{s,m})$. At each time step of the simulation we project the atomic velocities on the set of vectors which spans this subspace. For topologically symmetric systems the INS spectra of $q_{c,m}, q_{s,m}$ and $\text{span}(q_{c,m}, q_{s,m})$ coincide (e.g., Figure 1b, n, and q and a, e, and m).

Note that this technique can only be used for single closed ring systems, and it is not expected to completely resolve spectra in systems with fused rings. If multiple rings are attached to each other, then one has to distinguish between them to make use of the circulant matrix as a model for the Hessian. This is still useful because the resulting spectra can be directly compared with spectra from other n -ring structures. In this way the immediate effect of a different topology on a specific structure can be studied.

■ RESULTS AND DISCUSSION

Figure 1 gives an overview of the three-dimensional (3D) optimized geometries of the simulated structures. Some of them are key components of the MFI structure, and others have been suggested to occur in the early stages of other zeolite structures.²⁶ The initial geometry as input for the MD simulation does not need to coincide with the global minimum as all possible structures on the PES will be visited during the MD run. The most elementary structures are a single four-, five- and six-membered ring (Figure 1a, e, and m), and their spectra may be regarded as reference. Larger building blocks can be constructed by connecting these elementary rings with other n -ring structures. These new structures yield new (partial) INS spectra which can be compared with the reference spectra, and such an investigation provides us information on the influence of the topology (i.e., how atoms are linked to each other) on the vibrational spectra. In the synthesis of zeolites with MFI topology it has been found that the five-membered ring (5T) (Figure 1e), also called the pentasil ring, is of special importance.^{56–58} By connecting these pentasil rings larger building blocks can be constructed. If three T-atoms are added, then two 8T(2×5) (Figure 1k) and three 11T(3×5) (Figure 1h) sideways five-membered rings arise. If two sides of two different five rings are shared (sharing three T-atoms), then the 7T five ring is formed, 7T(2×5) (Figure 1j). The five ring 8T(4×5) (Figure 1l) is a silica octamer, where the rings form a cagelike structure. The species where two five rings do not share but are connected with an oxygen bridge is referred to as 10T(2×5) (Figure 1g). In this topology an extra six ring is present. Finally the silica dodecamer structure forms the 12T(4×5) (Figure 1i).²⁶

In aqueous silicate solutions the cubic octamer^{59,60} often has been observed experimentally and proposed as a building block. Therefore we also consider this full cube (6×4) (Figure 1q), a half cube (2×4) (Figure 1o), and a three-fourths cube (3×4) (Figure 1p).

Physical Meaning of IC's. The most basic molecular structures are the four-, five-, and six-rings (Figure 1a, e, and m, respectively). Their spectra may serve as a reference for other topologies where n_1 -rings are attached to n_2 -rings. In this way, the vibrational spectra can be applied as a tool for studying topological differences in zeolite structures (e.g., during nanogrowth).

Looking at the diagram of Figure 2, we can distinguish between two types of IC's: those that can be identified as single stretches and those that show a weighted mixture of stretch modes. For the first type of IC's it is straightforward to assign a physical motion to them since they coincide with real stretches. For the second type of IC's it is less straightforward, but they also represent a real physical combined vibration.

Symmetric and antisymmetric ring vibrations have been defined in eqs 11 and 12. When the atomic velocities are projected on these IC's, we gain knowledge on the magnitude of these combined modes relative to the full vibrational spectrum.

The antisymmetric motions represent modes where the O atom oscillates between two Si atoms. Their spectral lines are located at frequencies larger than 800 cm^{-1} and are discussed in subsection Classes for Internal Coordinates.

The characteristic internal modes of a molecular system are determined by the eigenvalue equation of the Hessian:

$$HE = \omega^2 \mathbf{ME} \quad (23)$$

Here H is the Hessian which contains the second derivatives of the potential energy with respect to the Cartesian coordinates, \mathbf{M} is the mass matrix, ω^2 represents the eigenvalues, and \mathbf{E} represents the $3N \times 3N$ matrix which contains the eigenvectors of the different modes (N = number of atoms). As shown in the Internal Coordinates Section, we introduced the circulant matrix as a model for the Hessian corresponding to the symmetric IC's and determined its eigenvectors and eigenvalues. The physical meaning of the combined modes of IC's $q_{c,m}$ and $q_{s,m}$ is interesting for further survey. For the four-, five-, and six-ring we have the following IC's (see eqs 22a and 22b) ($\alpha = 2\pi/n$):

- Four-ring: $q_{c,0}$, $\text{span}(q_{c,1}, q_{s,1})$, $q_{c,2}$ ($\alpha = 90^\circ$).
- Five-ring: $q_{c,0}$, $\text{span}(q_{c,1}, q_{s,1})$, $\text{span}(q_{c,2}, q_{s,2})$ ($\alpha = 72^\circ$).
- Six-ring: $q_{c,0}$, $\text{span}(q_{c,1}, q_{s,1})$, $\text{span}(q_{c,2}, q_{s,2})$, $q_{c,3}$ ($\alpha = 60^\circ$).

They all can be associated to a real physical mode. Consider, for example, the four-ring. When projecting on the corresponding IC's, the resulting spectral peaks agree with the molecular breathing motions, as depicted in Figure 5, in which an outward arrow means that the particular bond stretches out, whereas an inward arrow points to a shrinking motion of the bond. From this figure it is clear that $q_{c,1}$ and $q_{s,1}$ actually represent the same breathing mode, only shifted in phase by 90° . Thus, whenever a peak arises when projecting on a particular IC, we know with which vibrational eigenmode it corresponds. As a special combined mode we define in this work the breathing mode, in which all the present Si–O stretches are elongated or shrunk simultaneously. Here the mode $q_{c,0}$ represents this breathing mode.

Elementary Building Blocks: Four-, Five-, and Six-Rings. The spectra of all structures considered in this paper for all IC's are taken up in the Supporting Information. In this section some relevant spectra of the four-, five-, and six-rings are shown and will be further explained. We will focus on the spectral shifts that occur when spectra of the four-, five-, and six-rings for the same type of IC are compared. The conclusions that are drawn from these elementary structures are transferable to more complex molecular structures. Also for the sake of completeness INS and IR spectra for the four-, five-, and six-membered ring systems are given in the Supporting Information. They can serve as comparative material when analyzing velocity power spectra associated to specific IC's.

Terminal O–Si and Antisymmetric IC's. The spectra of the terminal O–Si and antisymmetric IC's are shown in Figure 6 for

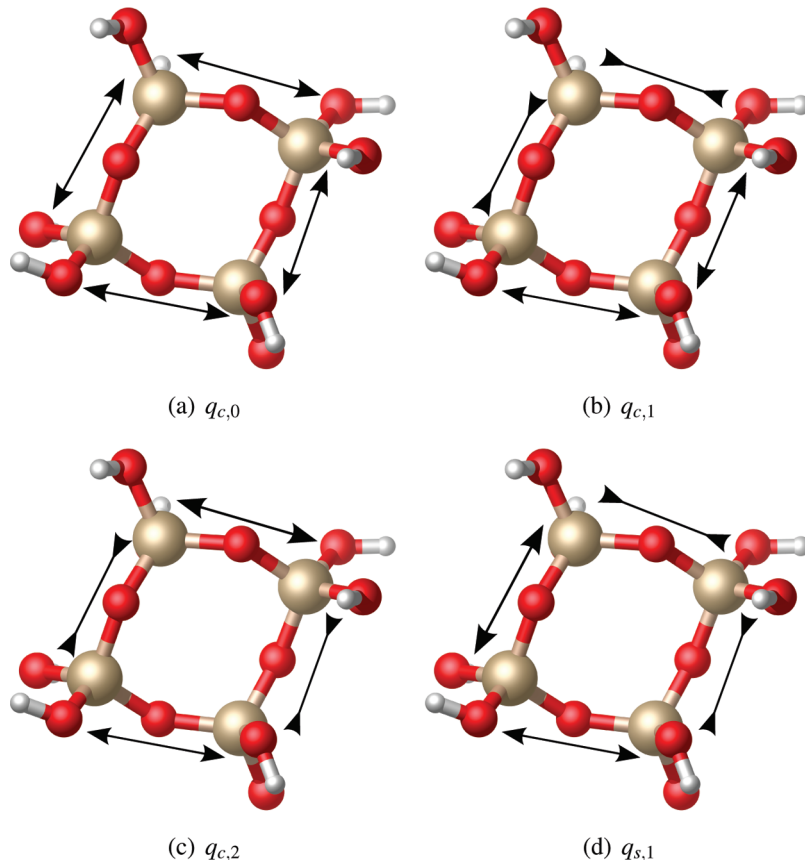


Figure 5. Visualization of the physical breathing modes when projecting atomic velocities on eigenvectors of the circulant matrix as a model for the Hessian.

the three elementary structures. For these classes of stretches multiple IC's are present. Per category the average spectrum is taken, as the spectra belonging to each IC of the same class are in essence not deviating much from each other. Also the standard deviation (stdev) of this average is given (lower curve). For both types of IC's the spectra manifestly show little influence on the size of the ring (same position, relative amplitudes, and shape).

Circulant Symmetric IC's. As outlined in the Method Section, the symmetric IC's are analyzed making use of the properties of the circulant matrix as a model for the Hessian. The spectra of the velocity projections on the $q_{c,m}$ and $q_{s,m}$ IC's of the four-, five-, and six-ring are shown in Figures 7 and 8. From these figures, some interesting features related to ring size can be derived.

- Comparing the first eigenmode, $q_{c,0}$, of the four, five-, and six-ring we see that the spectra of this breathing mode only exhibit a very small spectral shift which is almost negligible. The spectrum of the four-ring has peaks at 549 and 888 cm^{-1} , and for the five- and six-rings, we get 553 and 887 cm^{-1} and 562 cm^{-1} and 888 cm^{-1} , respectively. A small third peak emerges at about 453 cm^{-1} when increasing the size of the ring. It is at this stage not clear to which motion this third vibrational peak could be associated. The two peaks in the four-ring spectrum probably belong to the breathing modes of the ring Si and O atoms with a growing impact on the stretches. As the size of the ring increases, a collective nonplanar vibration could emerge. Although intuitive to some extent, these

explanations remain speculative as so far no visualization program is available which could remove this ambiguity.

- The peaks of the second mode of the four-ring, $\text{span}(q_{c,1}, q_{s,1})$, make a shift compared to the same mode of the five- and six-rings. The two peaks with the four-ring occur at 642 and 869 cm^{-1} , the five- and six-rings show peaks at 617 and 876 cm^{-1} and 602 and 881 cm^{-1} , respectively. There is some peak drift, and the interpeak distance grows with increasing ring size (red shift for the left peak, blue shift of the right peak). They are still relatively small but big enough to be measurable and to conclude that there is a size dependence, which is more pronounced than in the $q_{c,0}$ mode.
- The above made conclusions are also valid when the eigenmode $\text{span}(q_{c,2}, q_{s,2})$ of the five- and six-rings are compared.
- The interpretation of the spectra for these elementary building blocks, however, is also valid when combinations of these structures are made, as can be seen from the figures taken up in Figure 12 and the Supporting Information, e.g., 7T(4,5), 8T(4,6), and 9T(5,6). There is a very small topology dependence for the $q_{c,0}$ mode, and the influence of the ring size is larger for higher order modes.

We can discuss now how far the above features agree with what has been published in literature. The independence of spectra of the $q_{c,0}$ breathing coordinate on the ring size contradicts results of previous modeling studies. These works have demonstrated a

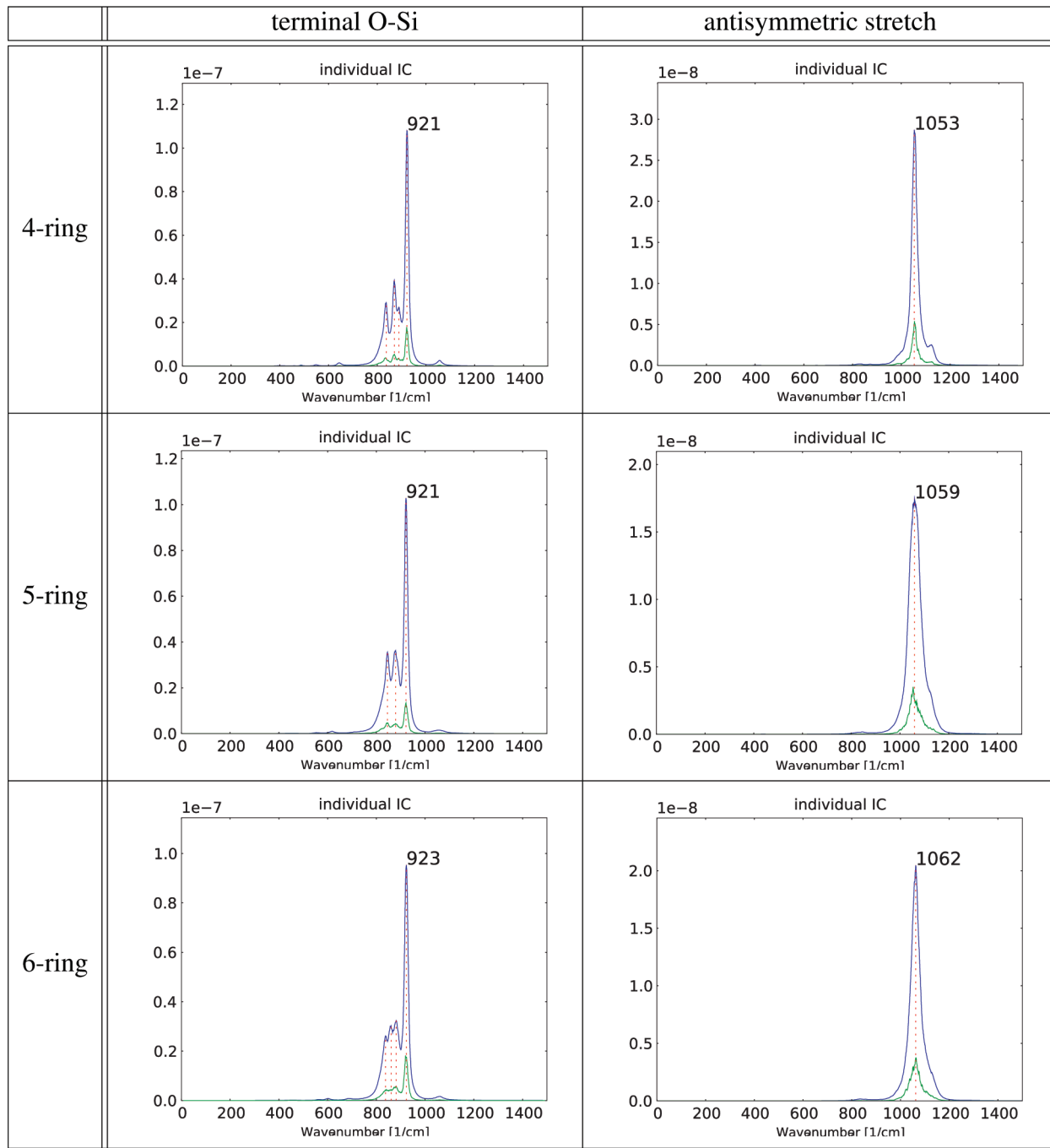


Figure 6. Projection of atomic velocities on the terminal O–Si and antisymmetric stretch IC's.

downward shift of the “ring breathing frequencies” with the increase of ring size. In the paper of Smirnov et al.³¹ the internal coordinate measuring the ring pore-opening has been put equal to

$$P(t) = \frac{1}{N/2} \sum_{i=1}^{N/2} R_i(t) \quad (24)$$

where $R_i(t)$ stands for the deviation of the i^{th} ring diameter from the mean value. The ring diameter is defined as the distance between oxygen atoms on the opposite sides of the ring. In order to comment on this issue, we have computed the velocity power spectrum of this vibrational coordinate $P(t)$ making use of the

MD results. These calculations could reveal the origin of the apparent discrepancies between the results presented in this work and those of literature. We also did the same exercise for the silica, instead of the oxygen atoms. The results are surprising and are displayed in Figure 9. Some peaks occurring in the $P(t)$ velocity power spectra for the silica atoms perfectly coincide with the q_{c0} in both four-, five-, and six-ring spectra. More specifically, four-ring: 550 and 892 cm^{-1} ; five-ring: 550 and 883 cm^{-1} ; and six-ring: 558 and 892 cm^{-1} . They do not show any ring size dependence. On the contrary, the oxygen $P(t)$ velocity power spectra do not show any resemblance with the q_{c0} , except perhaps for the spectral signal at 453 cm^{-1} appearing in six-membered rings. The downward shift of the ring breathing

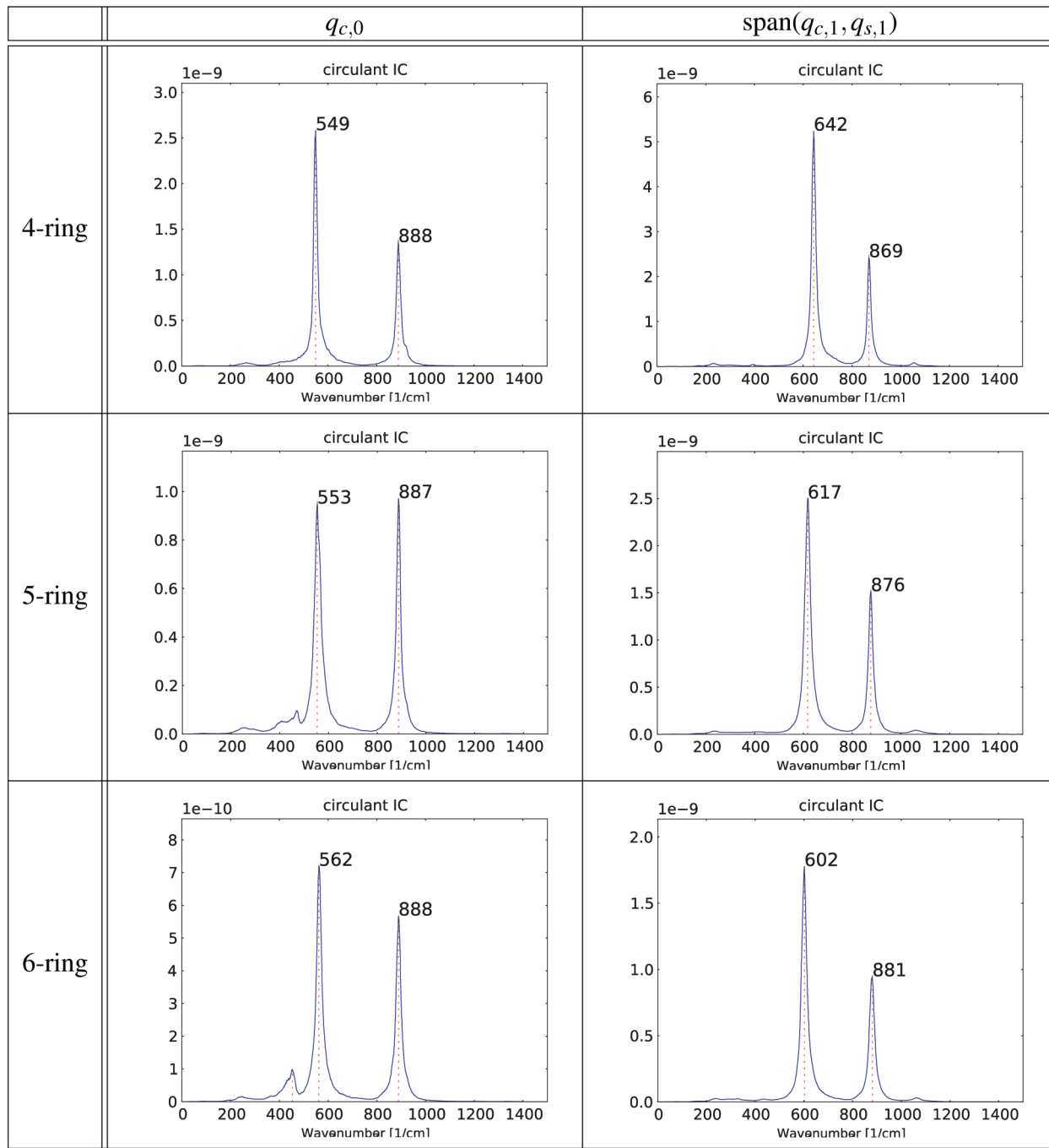


Figure 7. Projection of atomic velocities on the circulant symmetric IC's $q_{c,0}$ and $\text{span}(q_{c,1}, q_{s,1})$ for the four-, five-, and six-ring.

frequencies observed in literature is also reproduced in our $P(t)$ velocity power spectra for the oxygen atoms: 483, 475, and 458 cm^{-1} in going from four- to six-rings. They represent the lowest frequency peak in the spectrum. What can we conclude from this comparative study? Which peak corresponds really with the breathing mode where all ring diameter vibrations are supposed to be in phase? Since the pore-opening vibrational coordinate $P(t)$ does not take into account the phase of all ring diameter vibrations, the $P(t)$ velocity power spectra show admixtures of various ring modes, as shown in Figure 5 in case of a four-ring.

For completeness, we also introduced another internal coordinate being the sum of all O–O distances of neighboring oxygen bridges as suggested in ref 32. We adapted the velocity

projection method on this internal coordinate, and the resulting spectra are given in the Supporting Information. These spectra reveal a striking resemblance with previous $P(t)$ velocity power spectra both for the oxygen as for the silica atoms.

The presence of identical peaks in the three different types of power spectra (three different internal coordinates, namely $q_{c,0}$, $P(t)$ and $\sum R_{\text{O}-\text{O}}$) points manifestly toward a common vibrational mode, which represents probably the “true” breathing mode. However, to remove any ambiguity, we should be able to visualize the vibration corresponding to each peak in the power spectrum. But this is not an easy task and falls outside the scope of this work. Another aspect concerns the role of the force field used to perform the MD runs. It should be stressed that the fact that all

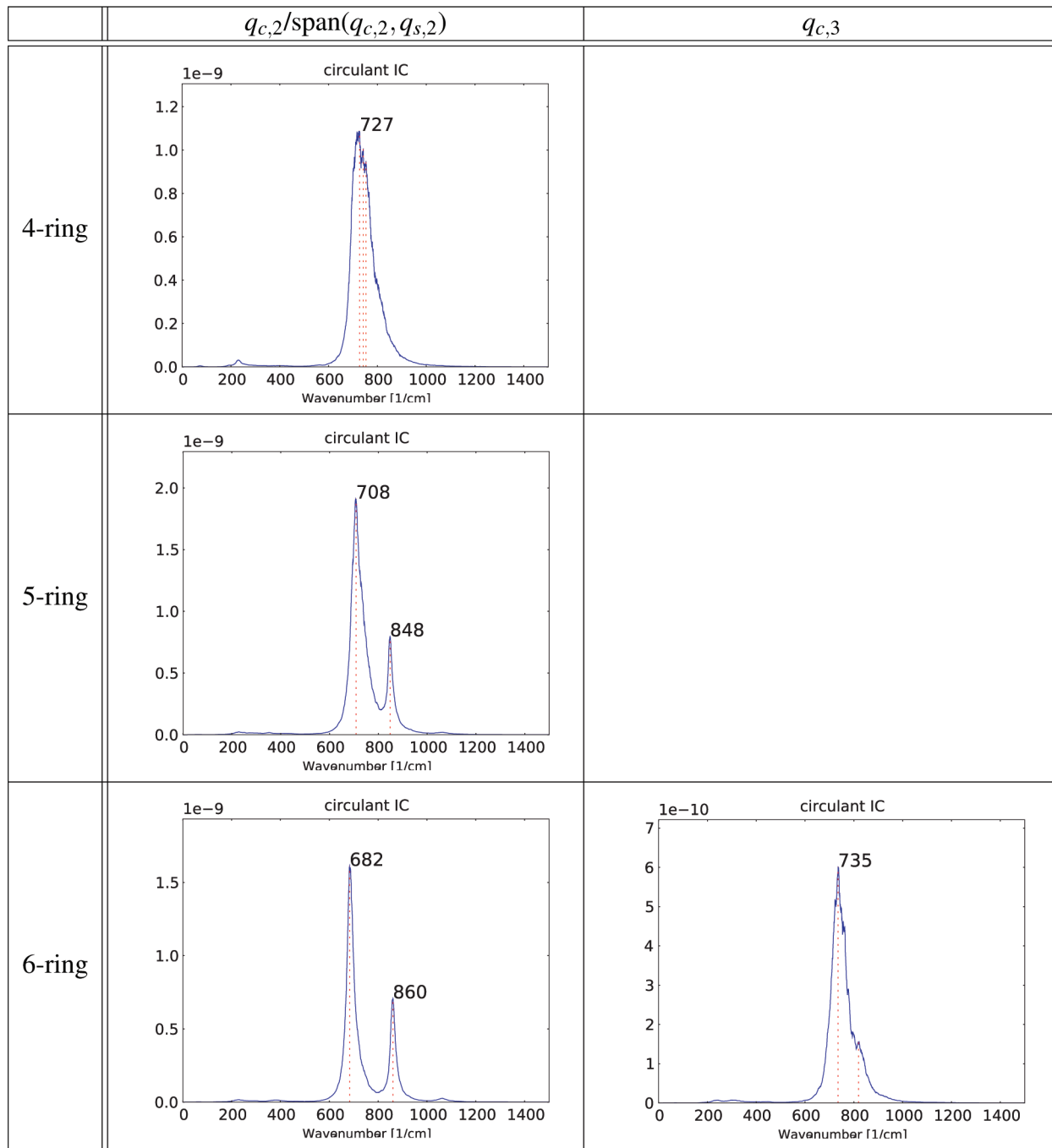


Figure 8. Projection of atomic velocities on the circulant symmetric IC's $q_{c,2}/\text{span}(q_{c,2}, q_{s,2})$ and $q_{c,3}$ for the four-, five-, and six-ring.

peaks observed in the $q_{c,0}$ spectra are also retrieved in the standard “non-projected” velocity power spectra corresponding with pore-opening IC's is a property independent of the choice of the force field. Use of another force field can reproduce the spectral lines at somewhat different wavenumbers and affects probably too the shift of a peak when increasing the ring size, but the general features, as sketched above, remain unaffected.

Projection on Orthogonal Basis of IC's and the Orthogonal Complement. In the previous section only one class of internal coordinates (O–Si stretches and linear combinations of them) has been investigated. In this section we want to see to what extent the restriction to this single class of stretches is accurate

enough. In other words what is the impact of the bending and dihedral motions on the vibrational spectra, or, more precisely, what is the impact of the remainder on the spectra after projecting out all tangent vectors belonging to stretches? The projection technique consists of determining all tangential atomic velocity vectors inducing a change in a particular IC. Modes induced by the normal components of the velocities are not considered as far as they do not belong to the entire class of IC's (stretches). For that reason we develop a method able to construct the so-called orthogonal complement of the basis of a given set of internal coordinates containing all the O–Si stretches (terminal O–Si + internal O–Si IC's). To obtain this orthogonal complement, the singular value decomposition of the

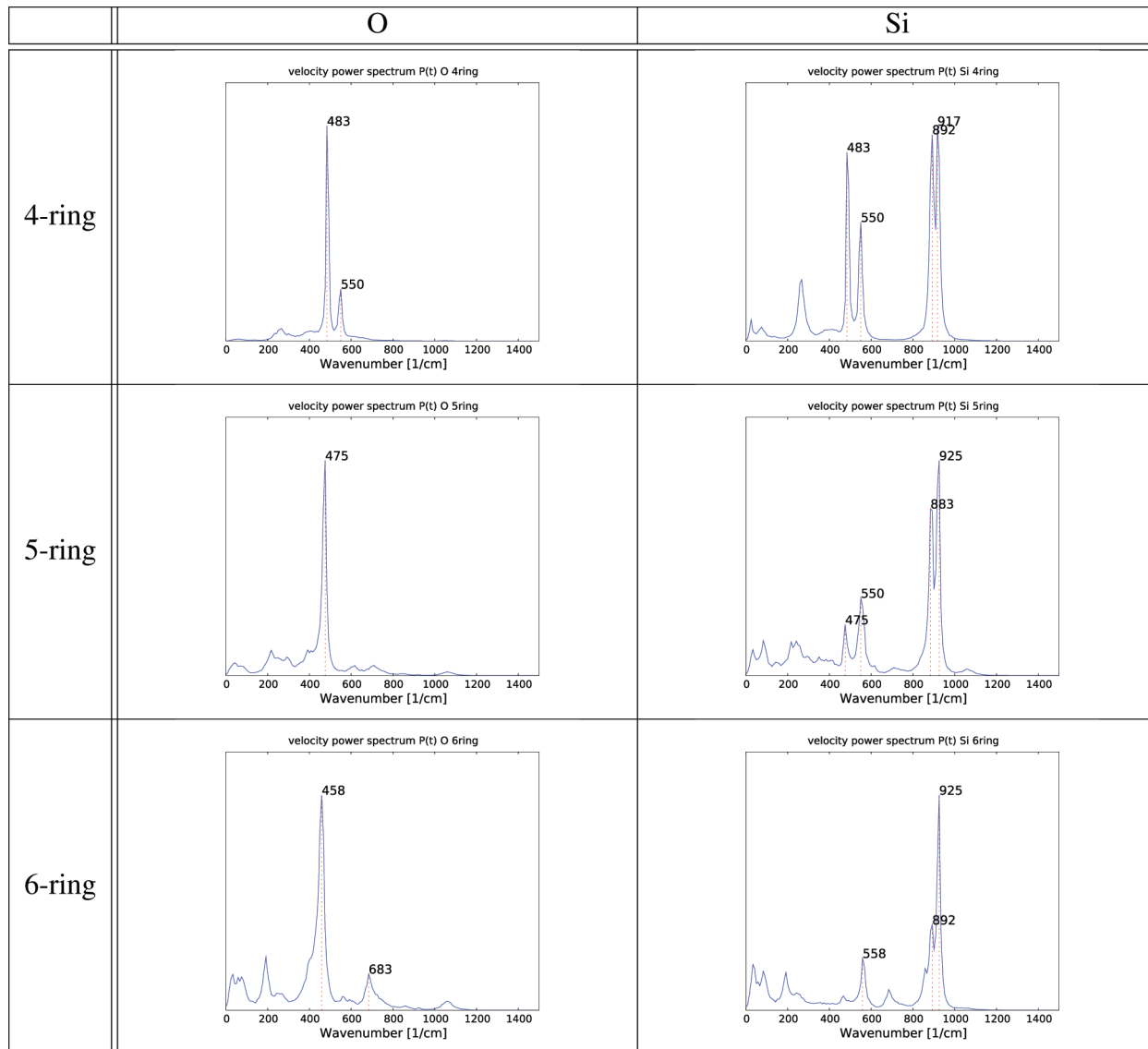


Figure 9. Velocity power spectra $P(t)$ for oxygen atoms as well as for silica and for the four-, five-, and six-rings.

matrix \mathbf{A} holding the tangent vectors of all the IC's is computed at every time step:

$$\mathbf{A}_{ki} = \frac{\partial q_k}{\partial x_i} \quad (25)$$

where $k = 1, \dots, K$ is an index characterizing the IC's, and the subscript $i = 1, \dots, 3N$ denotes the Cartesian coordinates. This procedure decomposes \mathbf{A} into three matrices:⁶¹

$$\mathbf{A} = \mathbf{U}\mathbf{W}\mathbf{V}^T \quad (26)$$

The matrices \mathbf{U} and \mathbf{V} are orthogonal, and \mathbf{W} has singular values and is diagonal. The first K columns of \mathbf{V} form an orthogonal basis for the IC's at each time step, while columns K to $3N$ construct the basis for the orthogonal complement at each time step. In a second step the atomic velocities are projected on both orthogonal bases. The result for the four-, five-, and six-rings is shown in Figure 10. The two full INS spectra are clearly well separated. The green spectrum ranging from 500 to 1200 cm^{-1} covers all O–Si stretches. The blue spectrum involves all IC modes belonging to the orthogonal complement, and for the

three-ring structures, all peaks are located below 500 cm^{-1} . This is a nice result as it demonstrates that our methodology works quite well in projecting out all bending and dihedral motions. The conclusion is that the frequency region in question between 500 – 1200 cm^{-1} is adequately probed by stretch IC's and that a one-to-one comparison with the full spectrum is possible. Analysis of the lower frequency spectrum should be done with care. The blue spectrum in Figure 10 grouping all IC's, excluding stretches, is a global spectrum. We did not project on the tangential vector of an individual IC belonging to the class of bending and dihedral angles. In principle the same procedure as in the previous subsection could be performed, but in view of the ultimate goal of this study, such investigation was expected to give little added value. Nevertheless additional information was extracted, which could be of interest. To illustrate with an example, we refer to the peak at around 25 cm^{-1} which is prominently present in the low-frequency spectra of the three-ring systems. This peak is probably due to a collective puckering mode of the ring, but as already stressed, a full treatment of the velocity projection protocol on

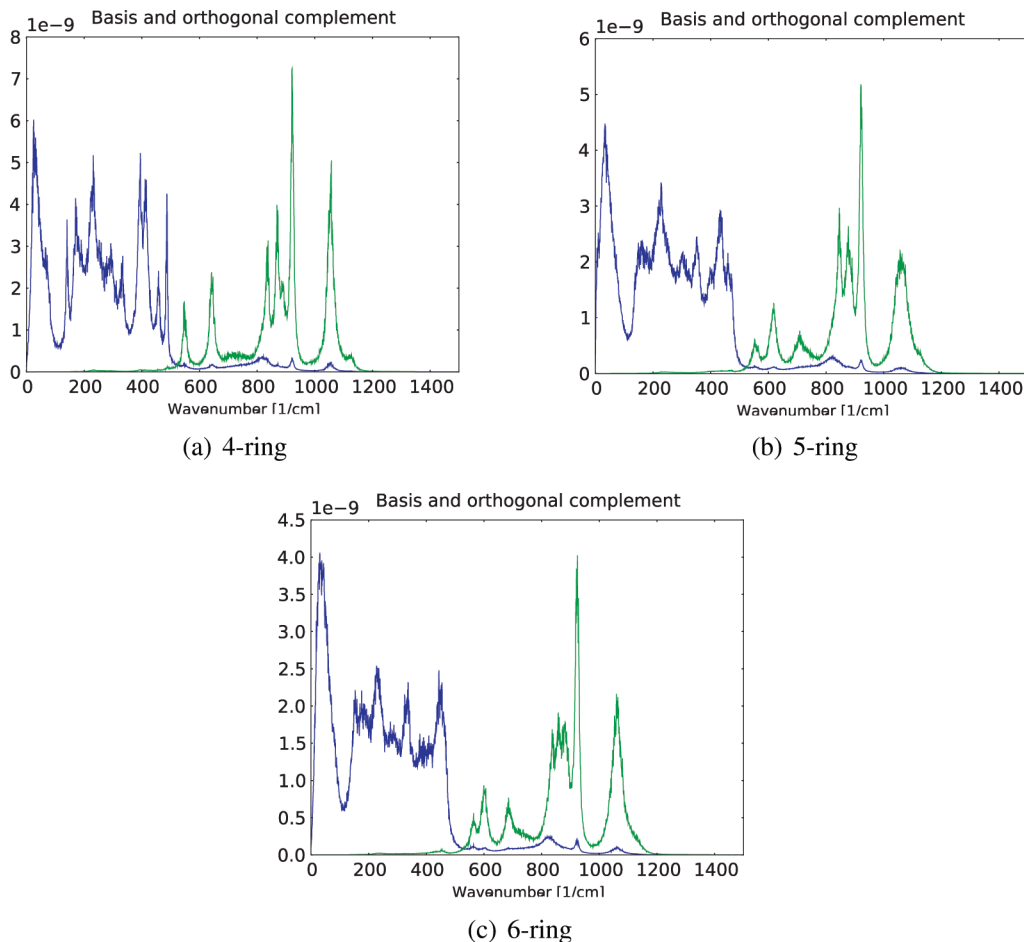


Figure 10. INS spectra of the projection of the atomic velocities on the basis of all O–Si IC’s (green curve) and on the orthogonal complement of these IC’s (blue curve).

the tangential vector of this puckering angle will reveal the real type of this specific mode.

Influence of the Connectivity. So far we studied the elementary four-, five-, and six-membered rings. We examined the influence of the sizes by comparing the spectra of them. Now we look at the connectivity (or the topology) by adding n -rings to these basic structures and investigate the corresponding fundamental changes in the spectra. In this section we will particularly focus on framework structures that contain five-membered rings (as in ref 26). Also the famous MFI-framework topology is built from five-membered rings. More precisely, in this section we will concentrate on the following ST ring clusters: 7T(2×5); 8T(2×5); 8T(4×5); and 11T(3×5) (see Figure 1). They all show two or more connected five-rings except for the reference five-membered ring. Each mode ($q_{c,0}$, $\text{span}(q_{c,1}, q_{s,1})$, and $\text{span}(q_{c,2}, q_{s,2})$) is more or less degenerate due to the appearance of multiple five-rings, hence an average is taken of the corresponding spectra. Spectra belonging to other building blocks are given in the Supporting Information.

As already observed for the elementary four-, five-, and six-membered rings, the ring size will not affect the INS spectra (see Supporting Information) for the terminal O–Si and antisymmetric IC’s. The changing topology induced by adding n -rings to elementary rings has no influence at all on the spectra; no peak shifts occur, and the shapes remain unaltered. This observation was more or less expected for the terminal O–Si stretches but

rather unexpected and even surprising for the antisymmetric stretch mode.

On the contrary, significant changes in the vibrational INS spectra occur for the various symmetric stretches. Spectra of the projected velocities on the circulant symmetric IC’s of the five-membered ring systems under study are shown in Figure 11.

All spectra are referred to with respect to the reference spectral lines observed for the elementary five-membered ring. Two connected five-rings sharing two atoms (8T(2×5), Figure 1k) cause a splitting of the two main peaks with a slight blue and red shift for the $q_{c,0}$ and $\text{span}(q_{c,1}, q_{s,1})$ mode. In principle two degenerate $q_{c,0}$ modes should exist. The slight coupling between these modes (for two rings share two silica atoms) gives rise to the observed small splitting. A third peak is manifestly present in the breathing mode $q_{c,0}$ and could be resolved by a suitable selection of an additional IC. The other connected five-ring structures lead to similar features. The 11T(3×5) structure with three connected five-rings shows the same pattern as the 8T(2×5), with the difference that now three five-rings are attached to each other which is reflected in the projected spectrum. In the 7T(2×5) structure the situation becomes more complex because now three Si atoms are shared. Since in the 8T(4×5) structure even more five-rings are shared, the spectra become more distinct from the reference single five-ring spectra. For the $\text{span}(q_{c,2}, q_{s,2})$ mode, the spectra show a remarkable resemblance in all structures. Another issue concerns

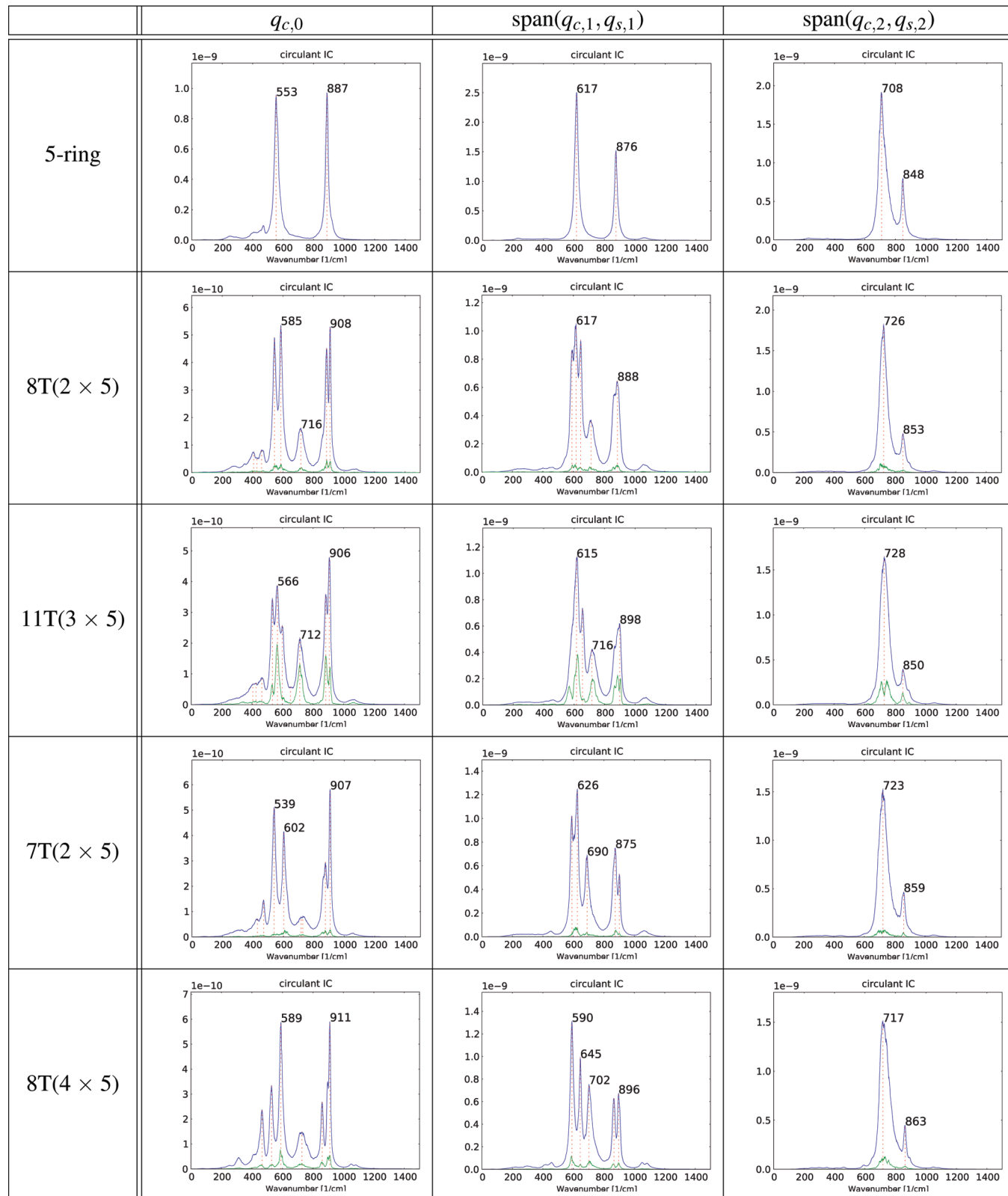


Figure 11. INS spectra belonging to atomic velocities projected on the circulant symmetric q_{ss} IC's for connected five-rings. Green curve: standard deviation.

the way spectra are affected by connecting rings of different sizes. We compare in Figure 12 the INS spectra generated by connecting a five-membered ring with, respectively, a four- and a six-

membered ring. Other spectra belonging to connected rings are shown in the Supporting Information. A common feature is the observation that when an n_2 -ring is attached to a basis n_1 -ring

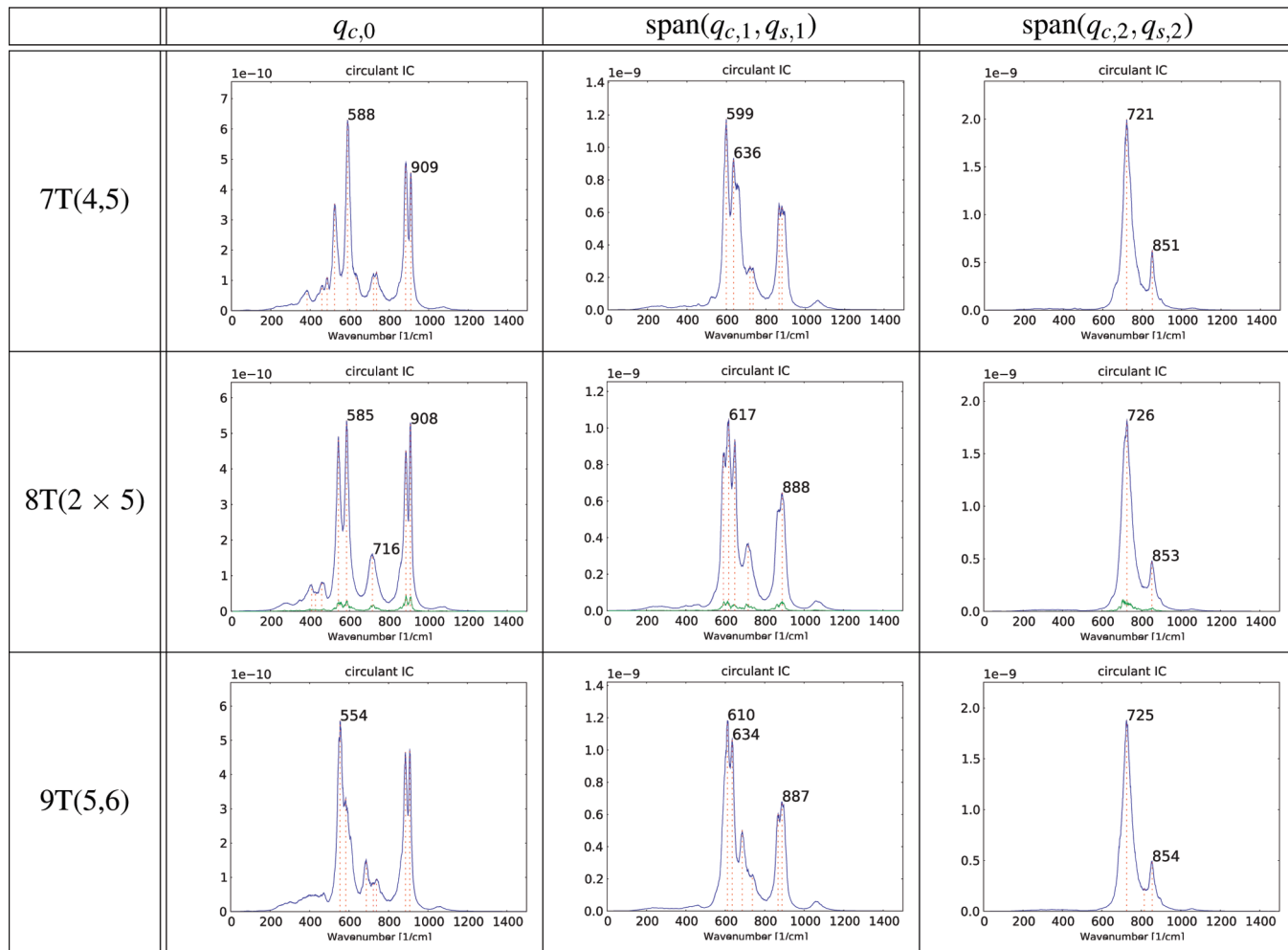


Figure 12. INS spectra belonging to atomic velocities projected on the circulant symmetric $q_{c,0}$ and $\text{span}(q_{c,1}, q_{s,1})$ and $\text{span}(q_{c,2}, q_{s,2})$ IC's for the five-ring connected with, respectively, a four-, five-, and six-ring.

($n_1 = 4-6$), the peaks of the $q_{c,0}$ and $\text{span}(q_{c,1}, q_{s,1})$ mode of the basis n_1 -ring seem to split up. One can distinguish between symmetrical ($n_1 = n_2$, e.g., five-ring attached to five-ring) and antisymmetrical splitting ($n_1 \neq n_2$, e.g., four-ring attached to five-ring). These effects are a logical result from the fact that the peaks of the modes of the n_1 - and n_2 -rings occur at the same frequency. When the two rings are attached, a resonance effect arises which causes one peak to turn into two floating modes: one peak with a slightly higher and one peak with a slightly lower wavenumber around the resonance frequency. When $n_1 = n_2$ the peaks show more or less the same amplitude, when $n_1 \neq n_2$ the difference in amplitude is much larger. Therefore it is useful to introduce the nomenclature of symmetrical and antisymmetrical splitting. An example is the 7T(2×5): the 553 and 887 cm^{-1} peaks of the five-ring split into $539, 602, 876$, and 907 cm^{-1} , respectively. Just as in the case of connecting five-rings, the $\text{span}(q_{c,2}, q_{s,2})$ mode remains the same.

The $q_{c,0}$ breathing mode is the most sensitive to connectivity differences. When more rings are attached to the elementary n_1 -rings, it is obvious that more peaks appear, since the ring systems cannot be regarded as independent systems anymore and mixing of modes occurs which results in extra peaks. This coupling gives rise to a splitting of the original peaks or the emerging of additional peaks. The $q_{c,0}$ mode is the most collective

mode because the breathing mode is determined by stretches which are not in an immediate antiphase (see Figure 5), giving this mode a more global character. The eigenmode of the $\text{span}(q_{c,2}, q_{s,2})$ IC on the other hand is the most local mode, as the successive stretches move in antiphase with each other (Figure 5). The topology dependence here is minimal.

It is important to note that the $q_{c,0}$ breathing mode is not affected by the size of the ring (see subsection "Circulant Symmetric IC's"), but is affected by the particular way in which it is connected to other rings.

CONCLUSION AND PERSPECTIVES

In this paper we have used the velocity projection method to assign (parts of) spectral peaks in zeolite vibrational spectra to particular changes in IC's. The focus was on essential zeolite building units, which can be assumed to play important roles during initial states of zeolite formation and during zeolite growth in general. The analysis of vibrational spectra can be a very useful tool in understanding the process, as the spectral behavior of eigenmodes of IC's can vary with different molecular systems. MD can then be used to simulate various structures which are key components during zeolite growth. The atomic velocities obtained from these MD runs can then be projected on a well chosen set of IC's.

Here, we focused on stretches, linear combinations of them, and eigenvectors of the circulant matrix as IC's. The circulant matrix was proposed as a model for the Hessian of ring molecular structures.

We found that the spectra of the terminal O–Si and the antisymmetric internal O–Si IC's were not influenced by the topology and by the size of the considered rings; the spectra of the elementary four,five-, and six-ring are the same. In addition, when other rings are attached to these basic n -rings, the same conclusions can be drawn.

When the atomic velocities are projected on the symmetric O–Si IC's, the resulting spectra differ for the four-,five-, and six-ring. The spectral shifts of the spectra of IC $q_{c,0}$ are tiny, while those corresponding with $\text{span}(q_{c,m}, q_{s,m})$ are rather substantial. The same trend can be observed in connected ring systems. We should, however, be very careful in drawing conclusions, as it is unclear what the role is of the force field in this specific field. It is recommended to refer to the spectra of the elementary rings when investigating the effect of connecting multiple n -rings. The most important conclusions are that the $q_{c,0}$ IC is the most sensitive mode to changes in molecular topology. It is the most global mode. We associate it to the breathing mode as it is determined by adjacent stretches which are not in antiphase. All the peaks occurring in the projected velocity $q_{c,0}$ power spectra are retrieved in power spectra belonging to other internal coordinates defining the ring-opening vibration.

About the connectivity we found that the size of the added n -rings does not play a crucial role; it is rather the way in which these rings are connected to each other that is the origin of the observed spectral changes.

When one projects the atomic velocities on the orthogonal complement of all stretch IC's present in a molecular structure, we found that the contribution of the stretch modes to the spectra is spectrally well separated from other contributions, like bending and dihedral angles. This confirms that the spectral region in which we are interested for zeolite synthesis can be almost completely resolved by considering changes in stretch modes.

In an attempt to decompose the spectra of the symmetric IC's further we introduced the circulant matrix as a model for the Hessian of the considered ring systems. If we want to extend the applications to systems which are not restricted to a ring structure, another more general approach is desired. A first incentive for this has already been found by linking the displacement (small motions) in IC's with the displacement (small motions) in Cartesian coordinates. We represent the displacement of the IC's by the $3N \times K$ matrix \mathbf{J}_{ik} (N is the number of atoms, K is number of IC's) and the Cartesian displacement by the $3N \times 3N$ matrix $\mathbf{E}_{i\lambda}$. The Cartesian eigenmodes can then be expanded in a redundant set of internal coordinates (they are not orthogonal) with $\alpha_{k\lambda}$ being the matrix which holds the expansion coefficients:

$$\sum_{k=1}^K \mathbf{J}_{ik} \alpha_{k\lambda} = \mathbf{E}_{i\lambda} \quad (27)$$

Here λ is a counter for the number of eigenmodes. The coefficients of the matrix $\alpha_{k\lambda}$ can then be used as coefficients for projecting the atomic velocities on the considered internal coordinates. The Cartesian eigenmodes $\mathbf{E}_{i\lambda}$ can only be obtained if the Hessian of the potential energy function is diagonalized, thus the mass-weighted normal mode eigenvalue equation has to be solved. To obtain the Hessian, a specified energy function V has to be provided. First results of this method were obtained, but it is still a work in progress.

APPENDIX

Eigenvalues and the k^{th} component of the normalized eigenvectors. We will show that component k of eigenvector m has the following form:

$$V_k^{(m)} = \exp\left(\frac{2\pi imk}{n}\right) \quad (28)$$

It is easy to see that the set of n orthogonal vectors $V^{(m)}$ with components of the form of eq 28, are eigenvectors of C . The product of C with $V^{(m)}$ can be written as

$$\begin{aligned} \sum_k C_{jk} V_k^{(m)} &= \sum_k c_{(j-k)} \exp\left(\frac{2\pi imk}{n}\right) \\ &= \sum_{k'} c_{(k')} \exp\left(\frac{2\pi im(j-k')}{n}\right) \\ &= \left[\sum_{k'} c_{(k')} \exp\left(\frac{-2\pi imk'}{n}\right) \right] \exp\left(\frac{2\pi imj}{n}\right) \\ &= \lambda^{(m)} V_j^{(m)} \end{aligned} \quad (29)$$

where the dummy summation index k was changed to $k' = (j - k) \bmod n$. It is clear that $V^{(m)}$ is indeed eigenvectors of the symmetric circulant matrix C .

The eigenvalues are real and can straightforwardly be rewritten as

$$\begin{aligned} \lambda^{(m)} &= \sum_k c_{(k)} \exp\left(\frac{-2\pi imk}{n}\right) \\ &= \sum_k \frac{1}{2} (c_{(k)} + c_{(-k)}) \exp\left(\frac{-2\pi imk}{n}\right) \\ &= \sum_k c_{(k)} \frac{1}{2} \left[\exp\left(\frac{-2\pi imk}{n}\right) + \exp\left(\frac{2\pi imk}{n}\right) \right] \\ &= \sum_k c_{(k)} \cos\left(\frac{2\pi mk}{n}\right) = \lambda^{(-m)} \end{aligned} \quad (30)$$

ASSOCIATED CONTENT

Supporting Information. Additional projected velocity power spectra, IR and INS spectra of all the oligomers are given. This material is available free of charge via the Internet at <http://pubs.acs.org>.

AUTHOR INFORMATION

Corresponding Author

E-mail: veronique.vanspeybroeck@ugent.be

ACKNOWLEDGMENT

This work is supported by the Fund for Scientific Research—Flanders (FWO), the Research Board of Ghent University (BOF) and BELSPO in the frame of IAP/6/27, the Belgian Prodex office, and ESA. Part of the computational resources and services used in this work were provided by Ghent University. V.

V.S. acknowledges the European Research Council under the European Community's Seventh Framework Programme (FP7-(2007-2013) ERC grant agreement no. 240483). J.A.M. acknowledges the Flemish government for long term structural funding (Methusalem).

■ REFERENCES

- (1) Boronat, M.; Viruela, P.; Corma, A. *J. Am. Chem. Soc.* **2003**, *126*, 3300–3309.
- (2) Nascimento, M. *J. Mol. Struct.* **1999**, *464*, 239–247.
- (3) Demontis, P.; Suffritti, G. *Chem. Rev.* **1997**, *97*, 2845–2878.
- (4) Hedlund, J.; Schoeman, B.; Sterte, J. *Progress in Zeolites and Microporous Materials*; Chon, H., Ihm, S.-K., Uh, Y. S., Eds.; Elsevier: Amsterdam, The Netherlands, 1997; pp 2203–2210.
- (5) Ravishankar, R.; Kirschhock, C.; Schoeman, B.; Vanoppen, P.; Grobet, P.; Storck, S.; Maier, W.; Schryver, F. D.; Martens, J.; Jacobs, P. *J. Phys. Chem. B* **1998**, *102*, 2633–2639.
- (6) Dokter, W.; van Garderen, H.; Beelen, T.; van Santen, R.; Bras, W. *Angew. Chem. Int. Ed.* **1995**, *34*, 73–75.
- (7) Knight, C.; Wang, J.; Kinrade, S. *Phys. Chem. Chem. Phys.* **2006**, *8*, 3099–3103.
- (8) Auerbach, S.; Monson, P.; Ford, M. *Curr. Opin. Colloid Interface Sci.* **2005**, *10*, 220–225.
- (9) Lewis, D.; Richard, C.; Catlow, A.; Thomas, J. *Faraday Discuss.* **1997**, *106*, 451–471.
- (10) Burkett, S.; Davis, M. *Chem. Mater.* **1995**, *7*, 920–928.
- (11) Corkery, R.; Ninham, B. *Zeolites* **1997**, *18*, 379–386.
- (12) Schoeman, B. *Microporous and Mesoporous Mater.* **1998**, *22*, 9–22.
- (13) Tsay, C.; Chiang, A. *Microporous Mesoporous Mater.* **1998**, *26*, 89–99.
- (14) Watson, J.; Brown, A.; Iton, L.; White, J. *J. Chem. Soc., Far Trans.* **1998**, *94*, 2181–2186.
- (15) de Moor, P.; Beelen, T.; van Santen, R.; Beck, L.; Davis, M. *J. Phys. Chem. B* **2000**, *104*, 7600–7611.
- (16) Li, Q.; Mihailova, B.; Creaser, D.; Sterte, J. *Microporous and Mesoporous Mater.* **2001**, *43*, 51–59.
- (17) Mintova, S.; Olson, N.; Senker, J.; Bein, T. *Angew. Chem., Int. Ed.* **2002**, *41*, 2558–2561.
- (18) Aerts, A.; Follens, L.; Haouas, M.; Caremans, T.; Delsuc, M.; Loppinet, B.; Vermant, J.; Goderis, B.; Taulelle, F.; Martens, J.; Kirschhock, C. *Chem. Mater.* **2007**, *19*, 3448–3454.
- (19) Kumar, S.; Davis, T.; Ramanan, H.; Penn, R.; Tsapatsis, M. *J. Phys. Chem. B* **2007**, *111*, 3398–3403.
- (20) Jin, L.; Auerbach, S.; Monson, P. *J. Phys. Chem. C* **2010**, *114*, 14393–14401.
- (21) Kirschhock, C.; Ravishankar, R.; Looveren, L. V.; Jacobs, P.; Martens, J. *J. Phys. Chem. B* **1999**, *103*, 4972–4978.
- (22) Kirschhock, C.; Ravishankar, R.; Verspeurt, F.; Grobets, P.; Jacobs, P.; Martens, J. *J. Phys. Chem. B* **1999**, *103*, 4965–4978.
- (23) Ravishankar, R.; Kirschhock, C.; Knops-Gerrits, P.; Feijen, E.; Grobet, P.; Vanoppen, P.; Schryver, F. D.; Miehe, G.; Fuess, H.; Schoeman, B.; Jacobs, P.; Martens, J. *J. Phys. Chem. B* **1999**, *103*, 4960–4964.
- (24) Verstraelen, T.; Szyja, B.; Lesthaeghe, D.; Declerck, R.; Van Speybroeck, V.; Waroquier, M.; Jansen, A.; Aerts, A.; Follens, L.; Martens, J.; Kirschhock, C.; van Santen, R. *Top. Catal.* **2009**, *52*, 1261–1271.
- (25) Petry, D.; Haouas, M.; Wong, S.; Aerts, A.; Kirschhock, C.; Martens, J.; Goskell, S.; Anderson, M.; Taulelle, F. *J. Phys. Chem. C* **2009**, *113*, 20827–20836.
- (26) Lesthaeghe, D.; Vansteenkiste, P.; Verstraelen, T.; Ghysels, A.; Kirschhock, C.; Martens, J.; Van Speybroeck, V.; Waroquier, M. *J. Phys. Chem. C* **2008**, *112*, 9186.
- (27) In *Normal mode analysis: theory and applications to biological and chemical systems*; Cui, Q., Bahar, I., Ed.; Chapman & Hall: Boca Raton, FL, 2006.
- (28) Scribano, Y.; Benoit, D. M. *J. Chem. Phys.* **2007**, *127*, 164118.
- (29) Bornhauser, P.; Calzaferri, G. *J. Phys. Chem.* **1996**, *100*, 2035–2044.
- (30) Pasquarello, A.; Car, R. *Phys. Rev. Lett.* **1998**, *80*, 5145–5147.
- (31) Smirnov, K.; Bougeard, D. *Catal. Today* **2001**, *70*, 243–253.
- (32) To, T.; Bougeard, D.; Smirnov, K. *J. Raman Spectrosc.* **2008**, *39*, 1869–1877.
- (33) Arab, M.; Bougeard, D.; Smirnov, K. *Phys. Chem. Chem. Phys.* **2002**, *4*, 1957–1963.
- (34) Jobic, H.; Smirnov, K.; Bougeard, D. *Chem. Phys. Lett.* **2001**, *344*, 147–153.
- (35) Smirnov, K.; Bougeard, D. *J. Raman Spectrosc.* **1993**, *24*, 255–257.
- (36) Smirnov, K.; Bougeard, D. *J. Phys. Chem.* **1993**, *97*, 9434–9440.
- (37) Smirnov, K.; Bougeard, D.; Maire, M. L.; Brémard, C. *Chem. Phys.* **1994**, *179*, 445–454.
- (38) Kuhne, T.; Krack, M.; Mohamed, F.; Parrinello, M. *Phys. Rev. Lett.* **2007**, *98*, 066401.
- (39) Kuhne, T.; Krack, M.; Parrinello, M. *J. Chem. Theory Comput.* **2009**, *5*, 235–241.
- (40) Jacob, C.; Reiher, M. *J. Chem. Phys.* **2009**, *130*, 084106.
- (41) Verstraelen, T.; Neck, D. V.; Ayers, P.; Speybroeck, V. V.; Waroquier, M. *J. Chem. Theory Comput.* **2007**, *3*, 1420.
- (42) Huang, Y.; Jiang, Z. *Microporous Mater.* **1997**, *12*, 341–345.
- (43) Flanigen, E.; Khatami, H.; Szymanski, H. In *Infrared Structural Studies of Zeolite Frameworks, Advances in Chemistry Series*; Flanigen, E. M., Sand, L. B., Eds.; American Chemical Society: Washington, D.C., 1974; Vol. 101.
- (44) de Man, A.; van Santen, R. *Zeolites* **1992**, *12*, 269–278.
- (45) van Santen, R.; Vogel, D. *Adv. Solid-State Chem.* **1989**, *1*, 151–224.
- (46) Wood, S. *J. R. Stat. Soc., B* **2000**, *62*, 413.
- (47) CP2K, 2008; <http://cp2k.berlios.de>.
- (48) Verstraelen, T.; Van Speybroeck, V.; Waroquier, M. *J. Chem. Inf. Mod.* **2008**, *48*, 1530–1541.
- (49) Verstraelen, T.; Van Houteghem, M.; Van Speybroeck, V.; Waroquier, M. *J. Chem. Inf. Mod.* **2008**, *48*, 2414.
- (50) Futrelle, R.; McGinty, D. *Chem. Phys. Lett.* **1971**, *12*, 285–287.
- (51) McQuarrie, D. In *Statistical mechanics*; Cato, R., Ed.; Harper & Row, 1976.
- (52) Berens, P.; Wilson, K. *J. Chem. Phys.* **1981**, *74*, 4872–4882.
- (53) Noid, D.; Koszykowski, M.; Marcus, R. *J. Chem. Phys.* **1977**, *67*, 404.
- (54) Papoulis, A. In *Probability, random variables and stochastic processes*; York, N., Ed.; McGraw-Hill, 1965.
- (55) Urey, H.; Bradley, C. *Phys. Rev.* **1931**, *38*, 1969–1978.
- (56) Watson, J.; Iton, L.; Keir, R.; Thomas, J.; Dowling, T.; White, J. *J. Phys. Chem. B* **1997**, *101*, 10094–10104.
- (57) Kragten, D.; Fedeyko, J.; Sawant, K.; Rimer, J.; Vlachos, D.; Lobo, R.; Tsapatsis, M. *J. Phys. Chem. B* **2003**, *107*, 10006–10016.
- (58) Mohamed, R.; Aly, H.; El-Shahat, M.; Ibrahim, I. *Microporous and Mesoporous Mater.* **2005**, *79*, 7–12.
- (59) Haouas, M.; Taulelle, F. *J. Phys. Chem. B* **2006**, *110*, 3007–3014.
- (60) Moravetski, V.; Hill, J.-R.; Eichler, U.; Cheetham, A.; Sauer, J. *J. Am. Chem. Soc.* **1996**, *118*, 13015–13020.
- (61) Press, W.; Teukolsky, S.; Vetterling, W.; Flannery, B. In *Numerical recipes in C: The art of scientific computing*; Press, W., Ed.; Cambridge University Press: New York, 1992.